# Thermosensitive transient receptor potential channels (thermo-TRPs) in human corneal epithelial cells

**Stefan Mergler**[1,*], **Fabian Garreis**[2], **Monika Sahlmüller**[1], **Peter S. Reinach**[3], **Friedrich Paulsen**[2], and **Uwe Pleyer**[1]

[1]Charité – Universitätsmedizin Berlin, Campus Virchow-Clinic, Department of Ophthalmology, Augustenburger Platz 1, 13353 Berlin, Germany

[2]Institute for Anatomy, LST II, University Erlangen-Nürnberg, Erlangen, Universitätsstraβe 19, Germany

[3]Department of Biological Sciences, State University of New York, College of Optometry, 33 West 42nd Street, New York, NY 10036, USA

## Abstract

Thermosensitive transient receptor potential proteins (TRPs) such as TRPV1-TRPV4 are all heat-activated non-selective cation channels that are modestly permeable to $Ca^{2+}$. TRPV1, TRPV3 and TRPV4 functional expression were previously identified in human corneal epithelial cells (HCEC). However, the membrane currents were not described underlying their activation by either selective agonists or thermal variation. This study characterized the membrane currents and $[Ca^{2+}]_i$ transients induced by thermal and agonist TRPV1 and 4 stimulation. TRPV1 and 4 expressions were confirmed by RT-PCR and TRPV2 transcripts were also detected. In fura2-loaded HCEC, a TRPV1-3 selective agonist, 100 µM 2-aminoethoxydiphenyl borate (2-APB), induced intracellular $Ca^{2+}$ transients and an increase in non-selective cation outward currents that were suppressed by ruthenium-red (RuR) (10–20 µM), a nonselective TRPV channel blocker. These changes were also elicited by rises in ambient temperature from 25 °C to over 40 °C. RuR (5 µM) and a selective TRPV1 channel blocker capsazepine (CPZ) (10 µM) or another related blocker, lanthanum chloride ($La^{3+}$) (100 µM) suppressed these temperature-induced $Ca^{2+}$ increases. Planar patch-clamp technique was used to characterize the currents underlying $Ca^{2+}$ transients. Increasing the temperature to over 40 °C induced reversible rises in non-selective cation currents. Moreover, a hypotonic challenge (25 %) increased non-selective cation currents confirming TRPV4 activity. We conclude that HCEC possess in addition to thermo-sensitive TRPV3 activity TRPV1, TRPV2 and TRPV4 activity. Their activation confers temperature sensitivity at the ocular surface, which may protect the cornea against such stress.

## Keywords

Human corneal epithelium; TRPV channels; intracellular $Ca^{2+}$; planar patch-clamping

[*]**Corresponding author:** Stefan Mergler, PhD, Charité – Universitätsmedizin Berlin, Campus Virchow-Clinic, Department of Ophthalmology, Augustenburger Platz 1, 13353 Berlin, Germany, Tel.: +49 (030) 450 559648, Fax: +49 (030) 450 559648, stefan.mergler@charite.de.

**Disclaimer**

The views, opinions and/or findings contained in this report are those of the author(s) and should not be construed as an official Department of the Army position, policy or decision, unless so designated by other official documentation. Citation of trade names in this report does not constitute an official Department of the Army endorsement or approval of the use of such commercial items.

## 1. Introduction

Normal vision depends on the maintenance of corneal transparency, which can be compromised if the outer and inner limiting epithelial and endothelial layers cannot offset the tendency of the stromal layer to imbibe fluid and swell. These limiting layers are able to counter stromal imbibition pressure by mediating net fluid flows into the tears and the aqueous humor. The bulk of the fluid outflow is attributable to endothelial function whereas the outer epithelial layer provides a fine tuning role. Under optimal conditions, epithelial fluid egress can contribute up to about 25% of the total dehydrating functions of the combined contributions by the epithelial and endothelial layers (Klyce, 1975). Another important attribute of the epithelium is its barrier function provided by the high resistance of tight junctions between closely apposed cells in the outer layers. The epithelial tight junction electrical resistance is much higher than that in the conjunctival layer (Ban et al, 2003;Yoshida et al, 2009). Its low permeability protects the tissue from environmental stresses such as pathogens that could lead to losses in transparency (Lu et al, 2001;Yoshida et al, 2009). Therefore, the maintenance of epithelial layer integrity is vital for preserving normal vision.

The cornea has a high density of sensory nerve endings that are unmyelinated and sensitive to touch, temperature and chemicals. The electrophysiological properties of primary sensory neurons innervating the cornea are attributable to the functional characteristics of their peripheral nerve terminals (Lopez de et al, 2000). In non-corneal cells, transient receptor potential channels (TRPs) participate in mediating responses to a number of stimuli that include temperature variation. In addition, these thermosensitive channels can be activated by capsaicin (CAP), menthol, 4 α PDD and 2-APB (Voets et al, 2005;McKemy et al, 2002;Peier et al, 2002;Reid, 2005). Recently, functional thermosensitive TRPV3 expression was described in human and murine corneal epithelial cells based on the calcium transients induced by a TRPV3 selective agonist (Yamada et al, 2009). However, there are no reports documenting corneal epithelial TRPV thermosensitive activity based on the effects of temperature variations on membrane currents.

The transient receptor potential (TRP) superfamily is subdivided into seven subfamilies: TRPC (canonical), TRPV (vanilloid), TRPM (melastatin), TRPP (polycystin), TRPA (ankyrin) and TRPML (mucolipin) on the basis of amino acid homology (Owsianik et al, 2005;Pedersen et al, 2005;Ramsey et al, 2006;Nilius et al, 2007). In addition, TRPN (NOMPC) channel proteins have been detected in nodose ganglia and in the gut wall from mice (Zhang et al, 2004) as well as in *Caenorhabditis elegans*, the fruit fly and zebra fish (Bodding, 2007). TRPs form homo- and heteromeric complexes whose $Ca^{2+}$ selectivity is variable. All of them are permeable to $Ca^{2+}$ except TRPM4 and TRPM5 whereas TRPV5 and TRPV6 are highly $Ca^{2+}$ permeable (Venkatachalam and Montell, 2007;Nilius et al, 2007).

TRP channel activity is regulated by both thermal and mechanical perturbations or through cell signaling linked to G-protein coupled receptors (GPCR's). TRPs contain thermo-TRPs such as TRPV1-6, TRPM8, and TRPA1. In contrast to TRPV1-4, the temperature sensitivity of TRPV5 and TRPV6 is relatively low (Nilius et al, 2007). Thermo-TRPs also function as chemosensors for a broad array of endogenous and synthetic ligands. Notably, TRPV1, which is also known as the capsaicin receptor, can alternatively be activated at room temperature when the proton concentration is increased (pH < 6) (Tominaga and Caterina, 2004). TRPV1 functional activity was detected in corneal epithelial cells since capsaicin-induced increases in proinflammatory cytokine release through transient $Ca^{2+}$ influx and activation of mitogen protein kinase (MAPK) signaling (Zhang et al, 2007). In a number of other tissues, TRPV1 activation occurs in response to heat (Bandell et al, 2004;Kochukov et

al, 2006;Numazaki and Tominaga, 2004;Pingle et al, 2007). Incidentally, some TRP family members are emerging as potential mechanosensitive channels that may underlie certain forms of mechanosensation in both sensory and nonsensory cells. For example, TRPV2 and TRPV4 are sensitive to hypotonic cell swelling, shear stress/fluid flow (TRPV4), and membrane stretch (TRPV2). TRPV4, which is also known as an osmosensor can be activated by mechanical stimuli (osmotic stress/stretch) and by diverse chemical compounds including 4 α-PDD and others (Vriens et al, 2007). Such TRPV4 activation was also detected in HCEC (Pan et al, 2008). A mechanosensitive role for the only mammalian TRPA family member, TRPA1, is beginning to emerge (O'Neil and Heller, 2005).

Thermosensitive-TRPs were identified in excitable and non-excitable cells. For example, TRPV4 has been described in endothelial cells and corneal epithelial cells (Fian et al, 2007;Hartmannsgruber et al, 2007;Kohler et al, 2006;Yao and Garland, 2005;Pan et al, 2008). TRPV3-4 expression was also observed in skin epidermal keratinocytes (Chung et al, 2003;Peier et al, 2002) and TRPV3 has been recently described in mouse distal colon epithelium and in the mouse cornea as well as in the HCEC (Ueda et al, 2009;Yamada et al, 2009). Notably, thermosensitive-TRPs such as TRPM8 are highly expressed in neuroendocrine tumor cells (Mergler et al, 2007), in LNCaP and PC-3 prostate cancer cells as well as in human prostate tissue (Bidaux et al, 2005;Thebault et al, 2005;Zhang and Barritt, 2004;Zhang and Barritt, 2006). Interestingly, TRPM8 could be also detected in human corneal endothelial cells. The role of this channel is still not elucidated (Mergler et al, 2005;Mergler and Pleyer, 2007). On the other hand, in HCEC epidermal growth factor (EGF) induces through EGFR phosphorylation TRPC4 activation, which is essential for optimal increases in cell proliferation (Yang et al, 2005). Even though there is some evidence for thermosensitive TRPV activity in HCEC, none of the TRPV- induced currents have yet been described that underlie increases in plasma membrane $Ca^{2+}$ influx.

We describe here in HCEC the membrane currents that underlie thermosensitive stimulation of TRPV1, 3 and 4 activity. The TRP channel modulators CAP, $La^{3+}$, RuR, CPZ and 2-APB as well as a hypotonic challenge were used to delineate the thermo-TRP channel subtypes. This study for the first time isolated the individual current contributions by TRPV1, 3 and 4 activation to $Ca^{2+}$ transients. Selective modulation of their activity entailed using pharmacological agents and defined temperature ranges.

## 2. Materials and Methods

### 2.1 Materials

Unless otherwise stated, all reagents were purchased from Sigma (Deisenhofen, Germany). 2-APB was purchased from Calbiochem (Merck Chemicals Ltd, Darmstadt, Germany). Medium and supplements for cell culture were purchased from GIBCO Invitrogen (Karlsruhe, Germany) or Biochrom AG (Berlin, Germany).

### 2.2 Cell culture

HCEC-SV40 were cultured as previously described (Pan et al, 2008;Zhang et al, 2007). In brief, HCEC were grown in Dulbecco's modified Eagle medium supplemented with 5% FCS, 20 µg/ml insulin, hydrocortisone and antibiotics. Cells were grown in a humidified atmosphere containing 5 % $CO_2$ at 37 °C. They were subcultivated by cell passage with accutase. Accutase activity was quenched with serum-supplemented growth medium. Cells were seeded on dishes and medium was changed three times per week.

### 2.3 RNA isolation and RT-PCR

Total RNA was extracted from confluent cultures of HCEC using TRIZOL® reagent (Invitrogen, Germany). Crude RNA was purified with isopropanol and repeated ethanol precipitation, DNA contamination was eliminated by digestion with RNase-free DNase I (30 min 37°C; Boehringer, Mannheim, Germany). The DNase was heat-inactivated for 10 min at 65°C. Reverse transcription of all RNA samples to first-strand cDNA was performed by RevertAid™ H Minus M-MuL V Reverse Transcriptase Kit (Fermentas, St. Leon-Rot, Germany) according to manufacturer's protocol. Two micrograms total RNA and 10 pmol Oligo $(dT)_{18}$ primer (Fermentas, St. Leon-Rot, Germany) were used for each reaction. In cDNA control samples, RevertAid™ H Minus M-MuL V reverse transcriptase was replaced with RNase- and DNase-free water. β-actin served as the internal control for the integrity of the transcribed cDNA.

Each PCR reaction contained in 20 µl, 1 µl cDNA mixture 2 µl 10× PCR buffer, 1 µl 50 mM $MgCl_2$, 1 µl 10 mM dNTPs mix (Fermentas, St. Leon-Rot, Germany), 0,5 µl 10 pmol forward primer, 0,5 µl 10 pmol reverse primer, and 0,2 µl (1,25 U) *Taq* DNA Polymerase (Invitrogen, Germany). Primers used were as follows: 5'-CTCCTACAACAGCCTGTAC-3' and 3'-AAGGCCTTCCTCATGCACT-5' for TRPV1 cDNA (Accession NM_018727), 5'-CTCTGGTGGCTAGCCTGTCCTGACA-3' and 3'-TGGGATCCCGGGAGCTTCTCA-5' for TRPV2 cDNA (Accession NM_016113) and 5′-ACTACGGCACCTATCGTCACCAC-3′ and 5′-ACGCTCAATGGCGATGTGC-3′ for TRPV4 cDNA (Accession NM_021625). The primers were synthesized at MWG-Biotech AG, Ebersberg, Germany. PCR reaction underwent an initial cycle at 95 °C for 5 min followed by 35 cycles of 95 °C for 15 s, Primer specific annealing temperatures used were: a) TRPV1 58 °C, b) TRPV2 64 °C and c) TRPV4 60,5 °C) for 30 s, followed by 72 °C for 45 s, and a final elongation at 72 °C for 7 min as well as a temperature hold at 4 °C. Ten microliters of the PCR product were loaded on a 1,5 % agarose gel and after electrophoresis they were visualized via fluorescence. Base pair (bp) values were compared with Genbank data. PCR products were also confirmed by sequencing (BigDye; Applied Biosystems, Foster City, CA).

### 2.4 Intracellular calcium fluorescence imaging

HCEC were pre-incubated with culture medium containing 2 µM fura-2-AM for 30 – 40 min at 37 °C. Thereafter, cells were washed with an extracellular sodium- and potassium-free bath solution containing 120 mM N-methyl-D-glucamine, 5.4 mM CsCl, 1 mM $MgCl_2$, 10 mM glucose, and 10 mM HEPES acid and 5 mM $CaCl_2$ (pH 7.3). $Ca^{2+}$ was the predominant charge carrier. Fura-2 fluorescence was measured at room temperature (≈ 20–23 °C) using a digital imaging system (T.I.L.L. Photonics, Munich, Germany) at 340 nm and 380 wavelengths, the ratio $(f_{340}/f_{380})$ is a relative index of changes in $[Ca^{2+}]_i$ (Grynkiewicz et al, 1985). If drugs were added from dimethyl sulfoxide (DMSO) containing stock solutions, the final solvent concentration did not exceed 0.1%. This solvent concentration did not influence fura-2 fluorescence in control experiments (data not shown).

### 2.5 Microchip technology for semi-automated patch-clamp recording

The whole-cell mode was used of a novel semi-automated patch-clamp having microchip technology (port-a-patch©) (Nanion, Munich, Germany) (Bruggemann et al, 2006;Bruggemann et al, 2008;Fertig et al, 2002;Pamir et al, 2008). In brief, cells in suspension were pipetted onto a microchip. Its resistance corresponds to a pipette resistance of 2 – 5 MΩ. Subsequently, suction was applied to move a cell onto the aperture. Suction pulses were then used to break open the cell membrane across the aperture, allowing formation of the whole-cell configuration. The standard external bath solution contained (in mM) NaCl (150), CsCl (6), $MgCl_2$ (1), $CaCl_2$ (1.5), glucose (10), and HEPES (10) at pH 7.4. For characterization of outward currents, NaCl was replaced by Na-gluconate. The

standard intracellular solution for whole-cell measurements contained (in mM) NaCl (150), $MgCl_2$ (3), EGTA (5), and HEPES (10) adjusted to 7.2 with NaOH. In experiments employing hypotonic stress, isotonic and hypotonic bath solutions consisted of (mM): NaCl (105), $MgCl_2$ (1), $CaCl_2$ (1), glucose (10), and HEPES (10), pH 7.4. The isotonic solution contained additionally 80 mM mannitol. The corresponding intracellular sodium-based solution contained (in mM) NaCl (150), $MgCl_2$ (1), $Na_2ATP$ (4), EGTA (5) and HEPES (10), pH adjusted to 7.2 with NaOH. To avoid any contribution by $Ca^{2+}$ flux, the seal enhancing solution was omitted since it contains a high $Ca^{2+}$ concentration. Membrane currents were recorded using an EPC 10 with Patchmaster version 2.5 for Windows (HEKA, Lamprecht, Germany). Membrane capacitance and access resistance were calculated with Patchmaster software. Mean access resistances of $20 \pm 2$ MΩ (n = 37) were observed in the whole-cell configuration. Series resistance errors as well as fast and slow capacity transients were compensated by the patch-clamp amplifier in connection with the software. All experiments were performed at room temperature ($\approx 20 - 23$ °C). Cells were characterized by applying voltage protocols and perfusion of appropriate compounds to study specific ion channel behavior (Bruggemann et al, 2006;Milligan et al, 2009). The holding potential (HP) was set to 0 mV to eliminate any possible contributions by voltage-dependent calcium channel activity. Notable, voltage-operated-calcium-channels (VOCCs) in HCEC could be activated at a holding potential of −70 mV (unpublished observation). Fast temperature increases from normal room temperature to > 40 °C were generated by heating the bath solution by application of heated extracellular solution. Current-voltage relations were obtained from voltage ramps from −60 to +130 mV (duration 500 msec). In addition, whole-cell currents were recorded for 400 ms using voltage steps ranging between −60 and +130 mV (10 mV increments). The resulting currents were normalized by the cell membrane capacitance (current density [pA/pF]). Plots were generated with SigmaPlot Software version 11 and electrophysiology module. Bar charts were plotted with GraphPad Prism version 5 for Windows (GraphPad Software, San Diego California USA). Unless otherwise stated, all two-dimensional diagrams were plotted with Origin version 8 for Windows (OriginLab Corporation, Northampton, MA, USA).

## 2.6 Data analyses and statistics

All values are reported as means ± SEM. The number of replicates is indicated in each case in brackets, near the traces (graphs) or bars. Statistical significance was determined with Student's *t*-test (parametric unpaired two-sample t-test) unless otherwise stated if the values were normally distributed according to Gaussian distribution. P values <0.05 (*) were considered as significant. Statistical tests were performed with SigmaStat version 3.5 for Windows (Systat Software, Inc.) and GraphPad Prism software version 5.0 (San Diego California USA).

# 3. Results

## 3.1 Cell size and morphology

Figure 1A shows fura-2 loaded HCEC in different cell densities prior to heat exposure that were alternately exposed to excitation wavelengths of 340 and 380 nm and viewed with emitted fluorescence at 510 nm. Cells were used in this configuration for calcium imaging and planar patch-clamp recordings. The same cells are shown in Fig. 1B following transient temperature elevation to 50 °C. Only a slight decrease in fluorescence intensity was detected. Fig. 1C shows the corresponding time course of the temperature variations during this experiment. Fig. 1D shows a HCEC micrograph of a suspension used for planar patch-clamp recordings at room temperature. A conventional microscope (Nikon) was used because the planar patch-clamp technique does not employ a microscope. For planar patch-clamping, cells are positioned and sealed onto the aperture by software-controlled

application of suction. No microscope or micromanipulator is needed. Interestingly, the calculated mean membrane capacitances $C_M$ of adherent cells for conventional patch-clamp recordings were higher than those for the planar patch-clamp measurements (conventional patch-clamp data not shown). Specifically, $C_M$ with the conventional patch-clamp was $87 \pm 14$ pF (n = 6) whereas $C_M$ determined with the planar patch-clamp was only $19 \pm 3$ pF (n = 37). Therefore, adherent HCEC grown on coverslips have larger cell surface areas than those in suspension corresponding to lower membrane current densities for adherent cells.

### 3.2 TRPV1, TRPV2, and TRPV4 gene expression in HCEC

Figure 2 shows that the anticipated PCR products for TRPV1 (285 bp), TRPV2 (228 bp), and TRPV4 (419 bp) were obtained based on the specific primer designs. The signals for TRPV1 were at higher levels than those for TRPV4 and TRPV2. The identity of the PCR products was confirmed by sequencing and sequence alignment (data not shown). Negative signals in the control reactions (Ø) performed without reverse transcriptase during cDNA synthesis confirmed specific amplification of only cDNA and excludes primer binding to genomic DNA. As a positive control, cDNA from brain was used. HCEC cDNA integrity/ stability was validated based on invariant and quality assessment of expression of β-actin as a housekeeping gene. In Fig. 2, β-actin PCR product as an internal standard is included. DNA ladder (M) lane and the other lanes (HCE, Ø and C) are shown from one typical PCR experiment/ ethidium bromide-stained agarose gel. Even though TRPV3 expression was described in HCEC, we refrained from probing for its expression (Yamada et al, 2009). As we previously demonstrated TRPV1 expression, its presence instead was used as the positive control (Zhang et al, 2007).

### 3.3 Thermo-TRP channel expression in HCEC

To test for functional expression of thermo-TRPs, we examined whether changes in bath solution temperature affect $f_{340nm}/f_{380nm}$ ratios. After incubating at $25.61 \pm 0.17$ °C ($\pm$ SEM; n = 10), a temperature increase to $43.20 \pm 1.10$ °C (n = 10) caused the $f_{340nm}/f_{380nm}$ ratio to rapidly rise within 1 min from $1.208 \pm 0.004$ to $1.446 \pm 0.059$ (n = 10; ***p = 0.0003) followed by recovery to its baseline level upon temperature reversal (Fig. 3A). This heat-induced ratio increase was less in the presence of either the non-selective TRP channel blockers lanthanum chloride ($La^{3+}$) (100 µM) ($1.203 \pm 0.012$; n = 4; **p = 0.0085) (Fig. 3C) or ruthenium-red (RuR, 10 µM) ($1.268 \pm 0.02$; n = 6; *p = 0.0125) (Fig. 4B). The smaller suppression by RuR suggests expression of different types of thermosensitive ion channels other than TRPV. The temperature variation range applied here included temperatures that selectively activate TRPV1 and TRPV3-4. Moreover, the heat-induced $[Ca^{2+}]_i$ increase was significantly reduced in the presence of the selective TRPV1 channel blocker capsazepine (CPZ) (10 µM) ($1.256 \pm 0.012$ n = 8; **p = 0.0021) specifically confirming TRPV1 expression. Application of 2-APB (500 µM) did not further increase the heat-induced $[Ca^{2+}]_i$ increase ($1.302 \pm 0.032$ n = 5; p > 0.05). Therefore, the effects of both heating and 2-APB were nonadditive.

To validate that extracellular $Ca^{2+}$ is necessary for the heat-induced increase in $[Ca^{2+}]_i$, we repeated the heat transient protocol after changing to a $Ca^{2+}$-free bath solution (1 mM EGTA). As expected, $_I f_{340}/f_{380}$ fell below the baseline in the $Ca^{2+}$ free solution ($1.091 \pm 0,027$; n = 5). After heating, the ratio remained unaltered ($1.102 \pm 0.035$; n = 5; p > 0.05) (Fig. 3B).

Interestingly, cold stimulation ($10.33 \pm 0.31$ °C; n = 4) caused a slight increase to $1.236 \pm 0.01$; n = 4, within 1 min suggesting slowing of metabolic activity. Subsequently, the ratio returned to baseline, sometimes even decreasing below it upon temperature reversal (Fig 3D). The summary of all experiments is shown in Figure 4D.

### 3.4 2-APB increased intracellular calcium through activation of TRPV channels

2-APB (100 µM) is a common activator of TRPV1, TRPV2, and TRPV3 (Hu et al, 2004). To determine if 2-APB increases $Ca^{2+}$ influx, 100 µM 2-APB was applied to the bath without simultaneous heating. 2-APB significantly increased the ratio from $1.203 \pm 0.033$ (baseline value, no drug, t = 200 sec) to $1.355 \pm 0.037$ at 380 sec (n = 12; **p < 0.005; paired t-test) (Fig. 5A). This 2-APB-induced $Ca^{2+}$ increase was reduced in the presence of RuR ($1.246 \pm 0.011$; n = 9; *p = 0.0228) (Fig. 5B). Therefore, the effect of 2-APB on $[Ca^{2+}]_i$ further indicates that there is thermosensitive TRPV1 and TRPV2 expression, which is consistent with their mRNA expression (Figure 2). The summary of all experiments is shown in Figure 5C. As 2-APB is not a selective TRPV1 agonist, we did not determine if 2-APB-increases of TRPV1-3 mediated $Ca^{2+}$ influx could be suppressed during exposure to CPZ.

### 3.5 Activation of different thermo TRPV channel subtypes by different level of heat stimulation

To further distinguish between different thermo TRPV channel subtypes in HCEC, cells were exposed to different elevated temperatures. In particular, we assayed the $Ca^{2+}$ responses after high heat stimulation ($49.9 \pm 0.5$ °C; n = 11) and low heat stimulation ($35.2 \pm 1.3$ °C; n = 4) with and without the nonselective TRPV channel blocker RuR (10 µM) (n = 3 – 5). With this protocol, contributions by TRPV3/TRPV4 and TRPV1 activation to $Ca^{2+}$ entry could be unraveled because these TRPs have definitive temperature activation thresholds; namely, at a high temperature induced larger $Ca^{2+}$ rises were greater than at a lower level. This clearly indicates additional activity attributable to other TRPVs besides TRPV1 after high heat stimulation (Fig. 6A–B). The applied temperatures did not reach as high as 52 °C which is needed for TRPV2 activation. As similarly shown in Fig. 4B, a reduction of the $Ca^{2+}$ responses could be detected at both low and high heat stimulation (Fig. 6C–E). However, a detailed analysis revealed that the effects of RuR were different at the two heat stimulation levels. Even though the inhibitory effect of RuR on putative TRPV3/TRPV4 channel activity is only evident at the beginning of low heat stimulation, the inhibitory effect of RuR on additive TRPV1 channel activity is clearly evident after high heat stimulation. In summary, different thermosensitive TRPV subtypes could be distinguished by these specific temperature variations.

### 3.6 Identification of CAP-activated non-selective cation channel currents

To directly assess the ionic currents underlying thermosensitive variations in $Ca^{2+}$ influx, we used the whole-cell mode of the planar patch-clamp technique. The compositions of the extra- and intracellular solutions are provided in the methods section. The stimulation protocol and experimental design used to characterize cation channel activity are shown in Figure 7A–B. The holding potential was set to 0 mV to eliminate any possible contributions of voltage-dependent $Ca^{2+}$ currents. In order to characterize outward currents, sodium chloride was replaced by sodium-gluconate. This replacement of anions by a non-permeating ion (gluconate) is a frequently used identifier. Gluconate is impermeable for the cell membrane because of size restriction. Therefore, the contribution by chloride ionic flux to the whole-cell membrane currents can be determined in this manner. As clearly shown in Fig. 7, the replacement of extracellular chloride by gluconate in the extracellular solution did not inhibit the CAP-induced outward currents. Two independent experimental series were carried out (NaCl versus Na-gluconate, Fig. 7G). Specifically, the outward currents at 130 mV with NaCl in the external solution were $189 \pm 82$ pA/pF (n = 4) whereas the outward currents with Na-gluconate were not different ($277 \pm 43$ pA/pF; n = 5; p > 0.05, unpaired tested). In addition, the inward currents were also not changed ($93 \pm 54$ pA/pF (n = 4) versus $83 \pm 16$ pA/pF (n = 5; p > 0.05, unpaired tested). Without inhibition of outward currents, there was no depolarization of the membrane potential. Since the test conditions -except

replacement of chloride by gluconate- were not changed, there is every indication that the detected CAP-induced outward currents are mainly cationic currents and not a chloride conductance into the cell.

In the following set of experiments, the temperature was maximally raised to $\approx$ 45 °C. It was not practical to raise them higher because above this level most whole-cell planar patch-clamp recordings were unstable or seals even broke at temperatures > 50 °C). In response to a suitable temperature increase from 20 °C to > 40 °C, a rapid increase in non-selective cation channel outward and inward currents occurred (Fig. 8A–B). Fig 8C demonstrates current responses which were induced by a voltage ramp protocol from −60 mV to +130 mV (duration 500 msec). The summary of the voltage ramp experiments is shown in Fig. 8D–F. At −60 mV, the maximum nonselective cation inward currents rose to 130 $\pm$ 6 % of control (set to 100%) (p < 0.005; n = 14; paired tested). At 130 mV, the maximum nonselective cation inward currents rose to 132 $\pm$ 5 % of control (p < 0.005; n = 14; paired tested). To determine if the cells remained functional despite being exposed to high heat ($\approx$ 50 °C), we exposed the same cell to several pulses of this elevated temperature. As the heat-induced current increases were reproducible, the cells remained viable (under other ionic condition; data not shown). This indicates that short term exposures to $\approx$ 50 °C did not have injurious effects on cell function. Taken together, these results are consistent with the changes in fura-2 ratios induced by temperature variation and support the notion of functional expression of heat-sensitive, non-selective TRPV1-4 cation channels.

### 3.7 2-APB activates non-selective cation channel currents

Another approach to describe the currents underlying thermosensitive TRPV1-3 activation is to characterize changes induced by 100 µM 2-APB. Fig. 9A shows one typical experiment of current responses with and without 2-APB (100 µM) (voltage stimulation ramp protocol was used). The summary of the voltage ramp experiments is shown in Fig. 9B. At +130 mV, outward currents were transiently activated in the presence of 2 APB (142 $\pm$ 9 % of control; n = 6; p < 0.05; paired tested) whereas inward currents at −60 mV were not discernible in most recordings. Addition of 20 µM RuR moderately reduced these currents from 158 $\pm$ 12 % to 132 $\pm$ 12 % of control (100 %) (p < 0.05; both n = 3; paired tested) (Fig. 9C–F). As our fura-2 $Ca^{2+}$ imaging data replicate such sensitivity to 2-APB and RuR (Fig. 5), these experiments clearly show that there is TRPV1-3 channel activity in HCEC.

### 3.8 Hypotonic challenge activates non-selective cation channel currents

In response to hypo-osmotic stress ($\approx$ 233 mOsmol, leading to cell swelling and thus stretching of the plasma membrane), a rapid increase in non-selective cation channel outward and inward currents occurred (Fig. 10A–B). Fig 10C demonstrates current responses which were induced by a voltage ramp protocol as aforementioned. The summary of the voltage ramp experiments is shown in Fig. 10D–F. At −60 mV, the maximum nonselective cation inward currents rose to 143 $\pm$ 16 % of control (set to 100%) (p < 0.05; n = 9; paired tested). At 130 mV, the maximum nonselective cation inward currents rose to 138 $\pm$ 10 % of control (p < 0.01; n = 9; paired tested). Taken together, hypotonic stress-induced increases in TRPV4 activity resulted in elevated cation channel activity. This indicates the expression of functionally active TRPV4 channels in HCEC cells.

## 4. Discussion

Based on the results of RT-PCR, fluorescence calcium imaging and the planar patch-clamp technique, this study demonstrates that there is functional thermo-TRPV1, TRPV2 and TRPV4 expression in HCEC. TRPV1 and TRPV4 functional expression in HCEC was earlier described, but its thermosensitivity was not identified (Zhang et al, 2007;Pan et al,

2008). More recently, only thermosensitive TRPV3 elicited responses were described in this tissue (Yamada et al, 2009). However, none of these studies determined any of the increases in membrane current density that underlie elevations in intracellular $Ca^{2+}$ levels resulting from their activation. The current study dealt with these questions by characterizing both the membrane currents and changes in $f_{340nm}/f_{380nm}$ ratios induced by selective thermosensitive TRPV activation. Based on the differential effects of various agonists and antagonists as well as controlled reversible temperature elevations, the individual contributions were resolved by TRPV1-4 activation to these responses. The presence of such activity suggests that TRPV1-4 function is essential for corneal epithelial cells to withstand noxious rises in ambient temperature.

The heat-induced $Ca^{2+}$ transients and CAP-induced nonselective currents with a reversal potential of 0 mV are similar to those induced by CAP in HCEC (Zhang et al, 2007) and by heat in human corneal endothelial cells (Mergler et al, 2010). Considering the ion composition of the extra- and intracellular solutions, this reversal potential suggests that the non-selective ion channel is more cation than anion (e.g. $Cl^-$). Notably, replacing extracellular NaCl by Na-gluconate did not inhibit the CAP-induced outward currents indicating that there was no chloride conductance into the cell (Fig. 7). In all cases, the selective TRPV1 receptor antagonist CPZ blocked the $Ca^{2+}$ transients, which is consistent with what was described in cancer cells (Sanchez et al, 2005). Given this selectivity, described TRPV4 activity in HCEC was insensitive to CPZ (Pan et al, 2008). As thermosensitive TRPV1 activity was blocked in a $Ca^{2+}$-free medium, its activation depends on $Ca^{2+}$ in the extracellular medium. The non-selective cation current patterns resulting from TRPV1 activation are similar to those induced by capsaicin (Zhang et al, 2007) and TRPV1-transfected HEK293 cells (Voets et al, 2004). However, the current increases were less in HCEC than those in HEK293 cells probably because of higher TRPV1 receptor density in the transfected cells. A similar disparity exists in comparing cold-induced $Ca^{2+}$ increases in neuroendocrine tumor cells with those in TRPM8-transfected HEK293 cells. In this case, icilin was used as a cooling compound and the responses were greater in HEK293 (Mergler et al, 2007). In the current study, cooling induced a complex change in the $Ca^{2+}$ response pattern suggestive of TRPM8 expression (Fig. 3D). This is tenable because the response was similar to that induced by icilin in human synoviocytes, neuroendocrine tumor cells and human corneal endothelial cells (Kochukov et al, 2006;Mergler et al, 2005;Mergler et al, 2007). The suggested presence of TRPM8 could mean that this channel type interacts with TRPV1 as described in some non-corneal cells (Chuang et al, 2004;Voets et al, 2004).

The RT-PCR data shown in Figure 2 and the increased outward and inward currents by hypotonic challenge shown in Figure 10 validates TRPV4 expression. These results are also consistent with previously reported TRPV4 channel activity during exposure to a hypotonic challenge in HCEC as already demonstrated by us with calcium imaging experiments (Pan et al, 2008). Such expression has also been described in endothelial and renal epithelial cells (Hartmannsgruber et al, 2007;Kohler et al, 2006;Nilius et al, 2004;Wu et al, 2007). Even though the outward rectifying currents identified in planar patch-clamp recordings were larger than those described in the conventional patch-clamp recordings (Zhang et al, 2007), the current response patterns were comparable with one another. The higher current densities in the planar recordings may be due to the fact that with this technique the cells must be in suspension to obtain recordings. This technique is advantageous because it reduces both space-clamp problems and lowers membrane resistance (Bruggemann et al, 2006;Milligan et al, 2009). Accordingly, the current densities were greater with the planar patch-clamp configuration because of putative lower cell surface areas in cell suspension. Nevertheless, there is evidence that particular ion channel activities are unaltered by suspending the cells (e.g. epithelial sodium channels; data not shown). Furthermore planar

patch-clamping is advantageous because with this configuration stable seals are easier to obtain due to lower access resistances, which improves the quality of the cell recordings.

Other evidence for thermosensitive TRPV4 activity is that the TRPV channel blocker RuR reduced the heat-induced $Ca^{2+}$ increase (Fig. 4B, Fig. 6C). Although RuR blocks several TRPs including TRPV1-6, TRPA1, TRPM6 and TRPM8 (Ramsey et al, 2006), RuR was regularly used to block TRPV4 channel activity (Ducret et al, 2008;Jia et al, 2004;Kohler et al, 2006;Pan et al, 2008). We therefore assume that RuR blocks TRPV4 in HCEC as recently reported by Pan et al. 2008. The fact that $La^{3+}$ had a larger inhibitory effect than RuR (Fig. 3C versus Fig. 4B) indicates that other RuR insensitive channels are involved in the heat-induced $Ca^{2+}$ increase. Verification of thermosensitive TRPV4 expression in HCEC provides a drug target for preserving corneal epithelial function during exposure to a hypotonic challenge or a thermal stress.

In the whole-cell mode of the planar patch-clamp technique, hypotonic stress-induced outward rectifying currents and an increase of inward currents were registered. This is typical for TRPV4-like currents measured with relative low extracellular $Ca^{2+}$ (Fig. 10B–C). However, we generally observed moderate increases and outward rectifying. There are several possible reasons for this pattern. First of all, TRPV4 can be activated by exposing cells to hypotonicity, implying that this channel might be a cellular osmosensor (Nilius et al, 2004). In addition, reduced inward currents and strong outward rectification are associated with the presence of high extracellular $Ca^{2+}$ (e.g. 30 mM) (Nilius et al, 2004). In our study, we used only $1 – 1.5$ mM $Ca^{2+}$ which corresponds with clear inward current increases and moderate outward rectification as shown by Nilius et al (2004). TRPV4 activation by low heat (Fig. 7C–D) and by a hypotonic challenge (Fig. 10 B–C) showed current patterns which are typical for TRPV4-like currents. This corresponds with the $Ca^{2+}$ depending rectification of TRPV4 described in the literature (Nilius et al, 2003;Nilius et al, 2004;Voets et al, 2002). Another possibility is that as with TRPV1, TRPV4 expression levels may be at lower levels than those in other cell types or TRPV4-transfected cells.

The temperature range considered in this study limited us to probe for heat-induced activation of TRPV1 and TRPV3-4 channels. Over the range that we employed (Fig. 1C, Fig. 6A), we could resolve activation of: TRPV1 ($\geq 43$ °C), TRPV3 (33–39 °C) and TRPV4 (25–28 °C) (Venkatachalam and Montell, 2007;Tominaga and Caterina, 2004). Notably, the cells remained viable since the transient 50 °C heat-induced current increases were reproducible (data not shown). After reaching 50 °C, the heat-induced $Ca^{2+}$ increase recovered and cell morphology was unchanged (Fig. 1A–B,Fig. 6A). This indicates preservation of cell vitality at least under these conditions. That means that there was no damage to the cells by an irreversible increase in intracellular $Ca^{2+}$ and increased ion channel activity which is associated with cell apoptosis (Lu, 2006). Independently, the temperature was raised to $\approx 45$°C in our patch-clamp experiments because instable or broken seals at higher temperatures made whole-cell patch-clamp recordings impossible in most cases. Consequently, it was not possible to assess for TRPV2 involvement, which is activated by noxious heat ($\geq 52$ °C). It was also not possible to obtain recordings above 50 °C because of possible risk of cell damage and technical problems (e.g. unstable focus, RuR bleaching). Therefore, at the very least there is TRPV1, TRPV3 and TRPV4 functional expression in HCEC.

The changes induced by the TRP channel modulator 2-APB are reflective of TRPV1-3, but not TRPV4 activity (Ramsey et al, 2006). This agent has already been successfully used to probe for TRPV1-3 activation in non corneal cells (Chung et al, 2004;Colton and Zhu, 2007;Hu et al, 2004;Leffler et al, 2007). In HCEC, 2-APB evoked increases in $[Ca^{2+}]_i$, which were clearly suppressed in the presence of RuR suggesting TRPV1-3 channel activity

in HCEC (Fig. 5). The effects of 2-APB on intracellular $Ca^{2+}$ levels are consistent with our electrophysiological and RT-PCR data (Fig. 2, Fig. 9). Notably, the sensitivity of the 2-APB-induced current rise to blockage by RuR strongly indicates that $Ca^{2+}$ rather than $Cl^-$ influx underlies this increase. As our fura-2 $Ca^{2+}$ imaging data replicates such sensitivity to 2-APB and RuR, this agreement provides further evidence that the changes in channel activity are reflective of only TRPV subtype mediated influx. Interestingly, the heat-induced increases in non-selective cation channel currents were moderate compared to larger currents described in primary sensory cells (F-11 cells) and TRPV2-transfected HEK293 (Bender et al, 2005). Despite the smaller currents in HCEC, their patterns of activation may reflect also TRPV2 expression.

The presence of thermosensitive TRPV expression in HCEC may have physiological relevance as in vivo this tissue is exposed to daily temperature fluctuations. Such variability may be more pronounced in the avascular cornea than in other neighboring tissues receiving vascular supply. Even in a temperature controlled environment, the mean human corneal temperature range varies between 32 and 34 °C and decreases with age (Kocak et al, 1999). Such changes are principally related to changes in the tear film temperature (Purslow and Wolffsohn, 2007). In addition, temperature fluctuations can occur in different clinical settings. Heating the cornea above 40 °C (e.g. by laser treatment) is linked with thermal damage to the cornea (Mikesell, Jr. and Schepler, 1980). Similarly, corneal integrity may be challenged under eye bank storage conditions upon cooling the tissue to 4 °C. Regarding the biomechanical properties of the cornea, a temperature range of 30−50 °C does not change these properties (Sporl et al, 1996). On the other hand, cooling the cornea can prevent side effects of photorefractive keratectomy (Niizuma et al, 1994) and moderately cooled artificial tears provide relief to the eye by reducing corneal and conjunctival sensation (Fujishima et al, 1997). The identification of thermosensitive TRPV1, 3 and 4 activity provides insight into how the cornea can adapt to thermal stresses that are encountered in daily living.

Taken together, there is thermosensitive TRP1, 3 and 4 channel activity in HCEC. In addition, there is suggestive evidence for a TRPV2 counterpart. The presence of TRPV1 and 4 indicate that these channels are polymodal in that they are activated by temperature variations as well as eliciting increases in proinflammatory cytokine expression and regulatory volume behavior induced by exposure to capsaicin and a hypotonic challenge, respectively (Zhang et al, 2007;Pan et al, 2008). Moreover, we have convincing results that TRPV2 is also expressed in HCEC. The individual importance of these thermosensitive TRPV pathways to corneal homeostasis awaits clarification. This endeavor can be best undertaken once more selective modulators of their activity become available. Alternatively, the impact of specific TRPV gene deletions on corneal responses to thermal stress will resolve questions regarding the importance of TRPV function.

## Supplementary Material

Refer to Web version on PubMed Central for supplementary material.

## Acknowledgments

## Abbreviations

| | |
|---|---|
| **HCEC** | human corneal epithelial cells |
| **TRPV** | transient receptor potential vanilloid |
| **RuR** | ruthenium-red |
| **2-APB** | 2-aminoethoxydiphenyl borate |
| **CPZ** | capsazepine |
| **La$^{3+}$** | lanthanum chloride |

## Literature Cited

Ban Y, Dota A, Cooper LJ, Fullwood NJ, Nakamura T, Tsuzuki M, Mochida C, Kinoshita S. Tight junction-related protein expression and distribution in human corneal epithelium. Exp Eye Res. 2003; 76:663–669. [PubMed: 12742348]

Bandell M, Story GM, Hwang SW, Viswanath V, Eid SR, Petrus MJ, Earley TJ, Patapoutian A. Noxious cold ion channel TRPA1 is activated by pungent compounds and bradykinin. Neuron. 2004; 41:849–857. [PubMed: 15046718]

Bender FL, Mederos YS, Li Y, Ji A, Weihe E, Gudermann T, Schafer MK. The temperature-sensitive ion channel TRPV2 is endogenously expressed and functional in the primary sensory cell line F-11. Cell Physiol Biochem. 2005; 15:183–194. [PubMed: 15665528]

Bidaux G, Roudbaraki M, Merle C, Crqpin A, Delcourt P, Slomianny C, Thebault S, Bonnal JL, Benahmed M, Cabon F, Mauroy B, Prevarskaya N. Evidence for specific TRPM8 expression in human prostate secretory epithelial cells: functional androgen receptor requirement. Endocr Relat Cancer. 2005; 12:367–382. [PubMed: 15947109]

Bodding M. TRP proteins and cancer. Cell Signal. 2007; 19:617–624. [PubMed: 17029734]

Bruggemann A, Farre C, Haarmann C, Haythornthwaite A, Kreir M, Stoelzle S, George M, Fertig N. Planar patch clamp: advances in electrophysiology. Methods Mol Biol. 2008; 491:165–176. [PubMed: 18998092]

Bruggemann A, Stoelzle S, George M, Behrends JC, Fertig N. Microchip technology for automated and parallel patch-clamp recording. Small. 2006; 2:840–846. [PubMed: 17193131]

Chuang HH, Neuhausser WM, Julius D. The super-cooling agent icilin reveals a mechanism of coincidence detection by a temperature-sensitive TRP channel. Neuron. 2004; 43:859–869. [PubMed: 15363396]

Chung MK, Lee H, Caterina MJ. Warm temperatures activate TRPV4 in mouse 308 keratinocytes. J Biol Chem. 2003; 278:32037–32046. [PubMed: 12783886]

Chung MK, Lee H, Mizuno A, Suzuki M, Caterina MJ. 2-aminoethoxydiphenyl borate activates and sensitizes the heat-gated ion channel TRPV3. J Neurosci. 2004; 24:5177–5182. [PubMed: 15175387]

Colton CK, Zhu MX. 2-Aminoethoxydiphenyl borate as a common activator of TRPV1, TRPV2, and TRPV3 channels. Handb Exp Pharmacol. 2007:173–187. [PubMed: 17217057]

Ducret T, Guibert C, Marthan R, Savineau JP. Serotonin-induced activation of TRPV4-like current in rat intrapulmonary arterial smooth muscle cells. Cell Calcium. 2008; 43:315–323. [PubMed: 17669489]

Fertig N, Blick RH, Behrends JC. Whole cell patch clamp recording performed on a planar glass chip. Biophys J. 2002; 82:3056–3062. [PubMed: 12023228]

Fian R, Grasser E, Treiber F, Schmidt R, Niederl P, Rosker C. The contribution of TRPV4-mediated calcium signaling to calcium homeostasis in endothelial cells. J Recept Signal Transduct Res. 2007; 27:113–124. [PubMed: 17613724]

Fujishima H, Yagi Y, Shimazaki J, Tsubota K. Effects of artificial tear temperature on corneal sensation and subjective comfort. Cornea. 1997; 16:630–634. [PubMed: 9395871]

Grynkiewicz G, Poenie M, Tsien RY. A new generation of Ca2+ indicators with greatly improved fluorescence properties. J Biol Chem. 1985; 260:3440–3450. [PubMed: 3838314]

Hartmannsgruber V, Heyken WT, Kacik M, Kaistha A, Grgic I, Harteneck C, Liedtke W, Hoyer J, Kohler R. Arterial response to shear stress critically depends on endothelial TRPV4 expression. PLoS ONE. 2007; 2:e827. [PubMed: 17786199]

Hu HZ, Gu Q, Wang C, Colton CK, Tang J, Kinoshita-Kawada M, Lee LY, Wood JD, Zhu MX. 2-aminoethoxydiphenyl borate is a common activator of TRPV1, TRPV2, and TRPV3. J Biol Chem. 2004; 279:35741–35748. [PubMed: 15194687]

Jia Y, Wang X, Varty L, Rizzo CA, Yang R, Correll CC, Phelps PT, Egan RW, Hey JA. Functional TRPV4 channels are expressed in human airway smooth muscle cells. Am J Physiol Lung Cell Mol Physiol. 2004; 287:L272–L278. [PubMed: 15075247]

Klyce SD. Transport of Na, Cl, and water by the rabbit corneal epithelium at resting potential. Am J Physiol. 1975; 228:1446–1452. [PubMed: 165732]

Kocak I, Orgul S, Flammer J. Variability in the measurement of corneal temperature using a noncontact infrared thermometer. Ophthalmologica. 1999; 213:345–349. [PubMed: 10567864]

Kochukov MY, McNearney TA, Fu Y, Westlund KN. Thermosensitive TRP Ion Channels Mediate Cytosolic Calcium Response in Human Synoviocytes. Am J Physiol Cell Physiol. 2006

Kohler R, Heyken WT, Heinau P, Schubert R, Si H, Kacik M, Busch C, Grgic I, Maier T, Hoyer J. Evidence for a functional role of endothelial transient receptor potential V4 in shear stress-induced vasodilatation. Arterioscler Thromb Vasc Biol. 2006; 26:1495–1502. [PubMed: 16675722]

Leffler A, Linte RM, Nau C, Reeh P, Babes A. A high-threshold heat-activated channel in cultured rat dorsal root ganglion neurons resembles TRPV2 and is blocked by gadolinium. Eur J Neurosci. 2007; 26:12–22. [PubMed: 17596195]

Lopez de AM, Cabanes C, Belmonte C. Electrophysiological properties of identified trigeminal ganglion neurons innervating the cornea of the mouse. Neuroscience. 2000; 101:1109–1115. [PubMed: 11113359]

Lu L. Stress-induced corneal epithelial apoptosis mediated by K(+) channel activation. Prog Retin Eye Res. 2006; 25:515–538. [PubMed: 16962363]

Lu L, Reinach PS, Kao WW. Corneal epithelial wound healing. Exp Biol Med (Maywood ). 2001; 226:653–664. [PubMed: 11444101]

McKemy DD, Neuhausser WM, Julius D. Identification of a cold receptor reveals a general role for TRP channels in thermosensation. Nature. 2002; 416:52–58. [PubMed: 11882888]

Mergler S, Pleyer U. The human corneal endothelium: New insights into electrophysiology and ion channels. Prog Retin Eye Res. 2007; 26:359–378. [PubMed: 17446115]

Mergler S, Pleyer U, Reinach P, Bednarz J, Dannowski H, Engelmann K, Hartmann C, Yousif T. EGF suppresses hydrogen peroxide induced Ca2+ influx by inhibiting L-type channel activity in cultured human corneal endothelial cells. Exp Eye Res. 2005; 80:285–293. [PubMed: 15670807]

Mergler S, Strowski MZ, Kaiser S, Plath T, Giesecke Y, Neumann M, Hosokawa H, Kobayashi S, Langrehr J, Neuhaus P, Plockinger U, Wiedenmann B, Grotzinger C. Transient receptor potential channel TRPM8 agonists stimulate calcium influx and neurotensin secretion in neuroendocrine tumor cells. Neuroendocrinology. 2007; 85:81–92. [PubMed: 17426390]

Mergler S, Valtink M, Coulson-Thomas VJ, Lindemann D, Reinach PS, Engelmann K, Pleyer U. TRPV channels mediate temperature-sensing in human corneal endothelial cells. Exp Eye Res. 2010; 90:758–770. [PubMed: 20338165]

Mikesell GW Jr, Schepler KL. Implications of the corneal temperature range in the prediction of laser thermal damage. Am J Optom Physiol Opt. 1980; 57:228–235. [PubMed: 6770692]

Milligan CJ, Li J, Sukumar P, Majeed Y, Dallas ML, English A, Emery P, Porter KE, Smith AM, McFadzean I, Beccano-Kelly D, Bahnasi Y, Cheong A, Naylor J, Zeng F, Liu X, Gamper N, Jiang LH, Pearson HA, Peers C, Robertson B, Beech DJ. Robotic multiwell planar patch-clamp for native and primary mammalian cells. Nat Protoc. 2009; 4:244–255. [PubMed: 19197268]

Niizuma T, Ito S, Hayashi M, Futemma M, Utsumi T, Ohashi K. Cooling the cornea to prevent side effects of photorefractive keratectomy. J Refract Corneal Surg. 1994; 10:S262–S266. [PubMed: 7517314]

Nilius B, Owsianik G, Voets T, Peters JA. Transient receptor potential cation channels in disease. Physiol Rev. 2007; 87:165–217. [PubMed: 17237345]

Nilius B, Vriens J, Prenen J, Droogmans G, Voets T. TRPV4 calcium entry channel: a paradigm for gating diversity. Am J Physiol Cell Physiol. 2004; 286:C195–C205. [PubMed: 14707014]

Nilius B, Watanabe H, Vriens J. The TRPV4 channel: structure-function relationship and promiscuous gating behaviour. Pflugers Arch. 2003; 446:298–303. [PubMed: 12715179]

Numazaki M, Tominaga M. Nociception and TRP Channels. Curr Drug Targets CNS Neurol Disord. 2004; 3:479–485. [PubMed: 15578965]

O'Neil RG, Heller S. The mechanosensitive nature of TRPV channels. Pflugers Arch. 2005; 451:193–203. [PubMed: 15909178]

Owsianik G, Talavera K, Voets T, Nilius B. Permeation and Selectivity of TRP Channels. Annu Rev Physiol. 2005

Pamir E, George M, Fertig N, Benoit M. Planar patch-clamp force microscopy on living cells. Ultramicroscopy. 2008; 108:552–557. [PubMed: 17933465]

Pan Z, Yang H, Mergler S, Liu H, Tachado SD, Zhang F, Kao WW, Koziel H, Pleyer U, Reinach PS. Dependence of regulatory volume decrease on transient receptor potential vanilloid 4 (TRPV4) expression in human corneal epithelial cells. Cell Calcium. 2008; 44:374–385. [PubMed: 18355916]

Pedersen SF, Owsianik G, Nilius B. TRP channels: an overview. Cell Calcium. 2005; 38:233–252. [PubMed: 16098585]

Peier AM, Moqrich A, Hergarden AC, Reeve AJ, Andersson DA, Story GM, Earley TJ, Dragoni I, McIntyre P, Bevan S, Patapoutian A. A TRP channel that senses cold stimuli and menthol. Cell. 2002; 108:705–715. [PubMed: 11893340]

Pingle SC, Matta JA, Ahern GP. Capsaicin receptor: TRPV1 a promiscuous TRP channel. Handb Exp Pharmacol. 2007:155–171. [PubMed: 17217056]

Purslow C, Wolffsohn J. The relation between physical properties of the anterior eye and ocular surface temperature. Optom Vis Sci. 2007; 84:197–201. [PubMed: 17435533]

Ramsey IS, Delling M, Clapham DE. An introduction to TRP channels. Annu Rev Physiol. 2006; 68:619–647. [PubMed: 16460286]

Reid G. ThermoTRP channels and cold sensing: what are they really up to? Pflugers Archive. 2005; 451:250–263. [PubMed: 16075243]

Sanchez MG, Sanchez AM, Collado B, Malagarie-Cazenave S, Olea N, Carmena MJ, Prieto JC, Diaz-Laviada II. Expression of the transient receptor potential vanilloid 1 (TRPV1) in LNCaP and PC-3 prostate cancer cells and in human prostate tissue. Eur J Pharmacol. 2005; 515:20–27. [PubMed: 15913603]

Sporl E, Genth U, Schmalfuss K, Seiler T. Thermomechanical behavior of the cornea. Ger J Ophthalmol. 1996; 5:322–327. [PubMed: 9479512]

Thebault S, Lemonnier L, Bidaux G, Flourakis M, Bavencoffe A, Gordienko D, Roudbaraki M, Delcourt P, Panchin Y, Shuba Y, Skryma R, Prevarskaya N. Novel Role of Cold/Menthol-sensitive Transient Receptor Potential Melastatine Family Member 8 (TRPM8) in the Activation of Store-operated Channels in LNCaP Human Prostate Cancer Epithelial Cells. J Biol Chem. 2005; 280:39423–39435. [PubMed: 16174775]

Tominaga M, Caterina MJ. Thermosensation and pain. J Neurobiol. 2004; 61:3–12. [PubMed: 15362149]

Ueda T, Yamada T, Ugawa S, Ishida Y, Shimada S. TRPV3, a thermosensitive channel is expressed in mouse distal colon epithelium. Biochem Biophys Res Commun. 2009; 383:130–134. [PubMed: 19336223]

Venkatachalam K, Montell C. TRP channels. Annu Rev Biochem. 2007; 76:387–417. [PubMed: 17579562]

Voets T, Droogmans G, Wissenbach U, Janssens A, Flockerzi V, Nilius B. The principle of temperature-dependent gating in cold- and heat-sensitive TRP channels. Nature. 2004; 430:748–754. [PubMed: 15306801]

Voets T, Prenen J, Vriens J, Watanabe H, Janssens A, Wissenbach U, Bodding M, Droogmans G, Nilius B. Molecular determinants of permeation through the cation channel TRPV4. J Biol Chem. 2002; 277:33704–33710. [PubMed: 12093812]

Voets T, Talavera K, Owsianik G, Nilius B. Sensing with TRP channels. Nat Chem Biol. 2005; 1:85–92. [PubMed: 16408004]

Vriens J, Owsianik G, Janssens A, Voets T, Nilius B. Determinants of 4 alpha-phorbol sensitivity in transmembrane domains 3 and 4 of the cation channel TRPV4. J Biol Chem. 2007; 282:12796–12803. [PubMed: 17341586]

Wu L, Gao X, Brown RC, Heller S, O'Neil RG. Dual role of the TRPV4 channel as a sensor of flow and osmolality in renal epithelial cells. Am J Physiol Renal Physiol. 2007; 293:F1699–F1713. [PubMed: 17699550]

Yamada T, Ueda T, Ugawa S, Ishida Y, Imayasu M, Koyama S, Shimada S. Functional expression of transient receptor potential vanilloid 3 (TRPV3) in corneal epithelial cells: Involvement in thermosensation and wound healing. Exp Eye Res. 2009

Yang H, Mergler S, Sun X, Wang Z, Lu L, Bonanno JA, Pleyer U, Reinach PS. TRPC4 knockdown suppresses EGF-induced store operated channel activation and growth in human corneal epithelial cells. J Biol Chem. 2005; 280:32230–32237. [PubMed: 16033767]

Yao X, Garland CJ. Recent developments in vascular endothelial cell transient receptor potential channels. Circ Res. 2005; 97:853–863. [PubMed: 16254217]

Yoshida Y, Ban Y, Kinoshita S. Tight junction transmembrane protein claudin subtype expression and distribution in human corneal and conjunctival epithelium. Invest Ophthalmol Vis Sci. 2009; 50:2103–2108. [PubMed: 19117933]

Zhang F, Yang H, Wang Z, Mergler S, Liu H, Kawakita T, Tachado SD, Pan Z, Capo-Aponte JE, Pleyer U, Koziel H, Kao WW, Reinach PS. Transient receptor potential vanilloid 1 activation induces inflammatory cytokine release in corneal epithelium through MAPK signaling. J Cell Physiol. 2007; 213:730–739. [PubMed: 17508360]

Zhang L, Barritt GJ. Evidence that TRPM8 is an androgen-dependent Ca2+ channel required for the survival of prostate cancer cells. Cancer Res. 2004; 64:8365–8373. [PubMed: 15548706]

Zhang L, Barritt GJ. TRPM8 in prostate cancer cells: a potential diagnostic and prognostic marker with a secretory function? Endocr Relat Cancer. 2006; 13:27–38. [PubMed: 16601277]

Zhang L, Jones S, Brody K, Costa M, Brookes SJH. Thermosensitive transient receptor potential channels in vagal afferent neurons of the mouse. Am J Physiol Gastrointest Liver Physiol. 2004; 286:G983–G991. [PubMed: 14726308]
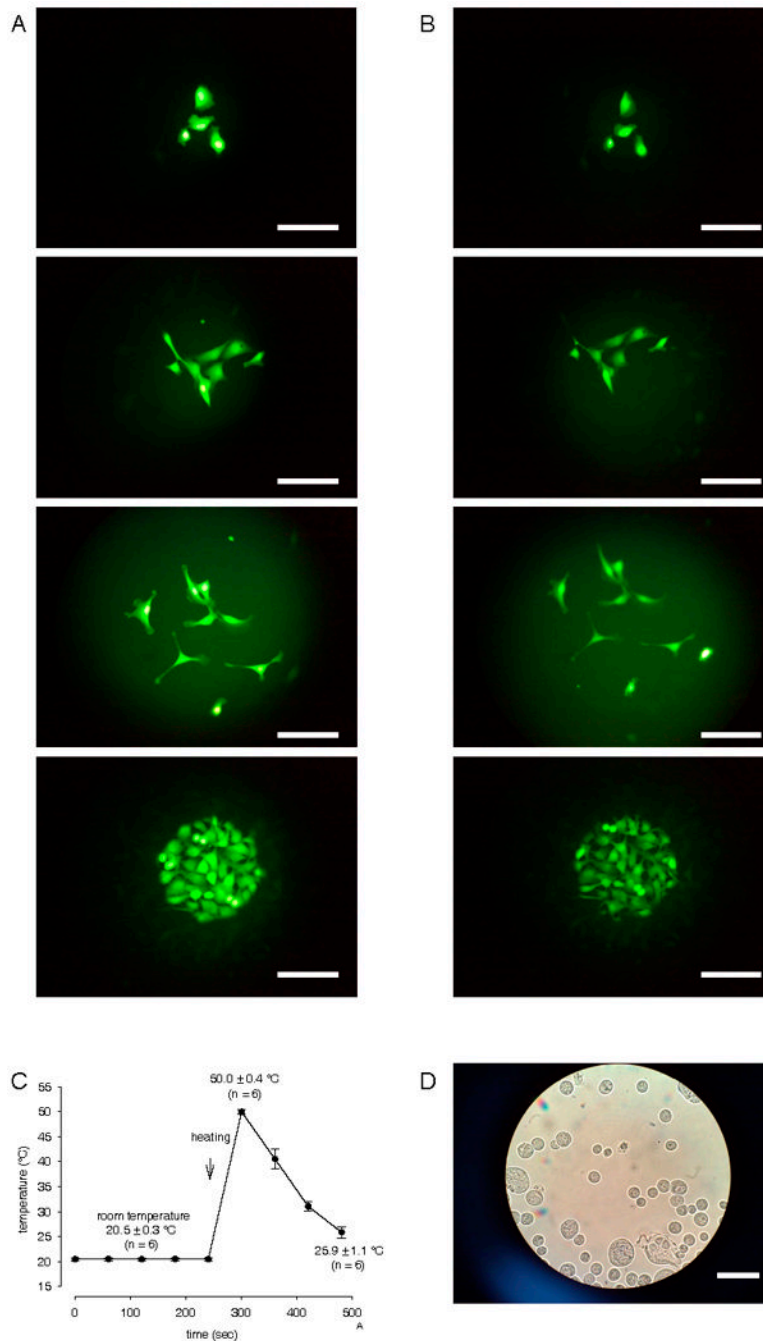
**Figure 1. HCEC micrograph**
(**A**) Fura-2 loaded HCEC in different cell densities viewed using fluorescence emission at 510 nm before high heat stimulation. Cells were used in this configuration to perform calcium imaging and obtain patch-clamp recordings. Scale bar is 50 µm. (**B**) Same HCEC but after heating stimulation demonstrating only a slight decrease in fluorescence intensity after high heat stimulation (until 50 °C). (**C**) Time dependent temperature variation protocol (n = 6). (**D**) Micrograph of HCEC in suspension as used for planar patch-clamp recordings. Scale bar is 30 µm.
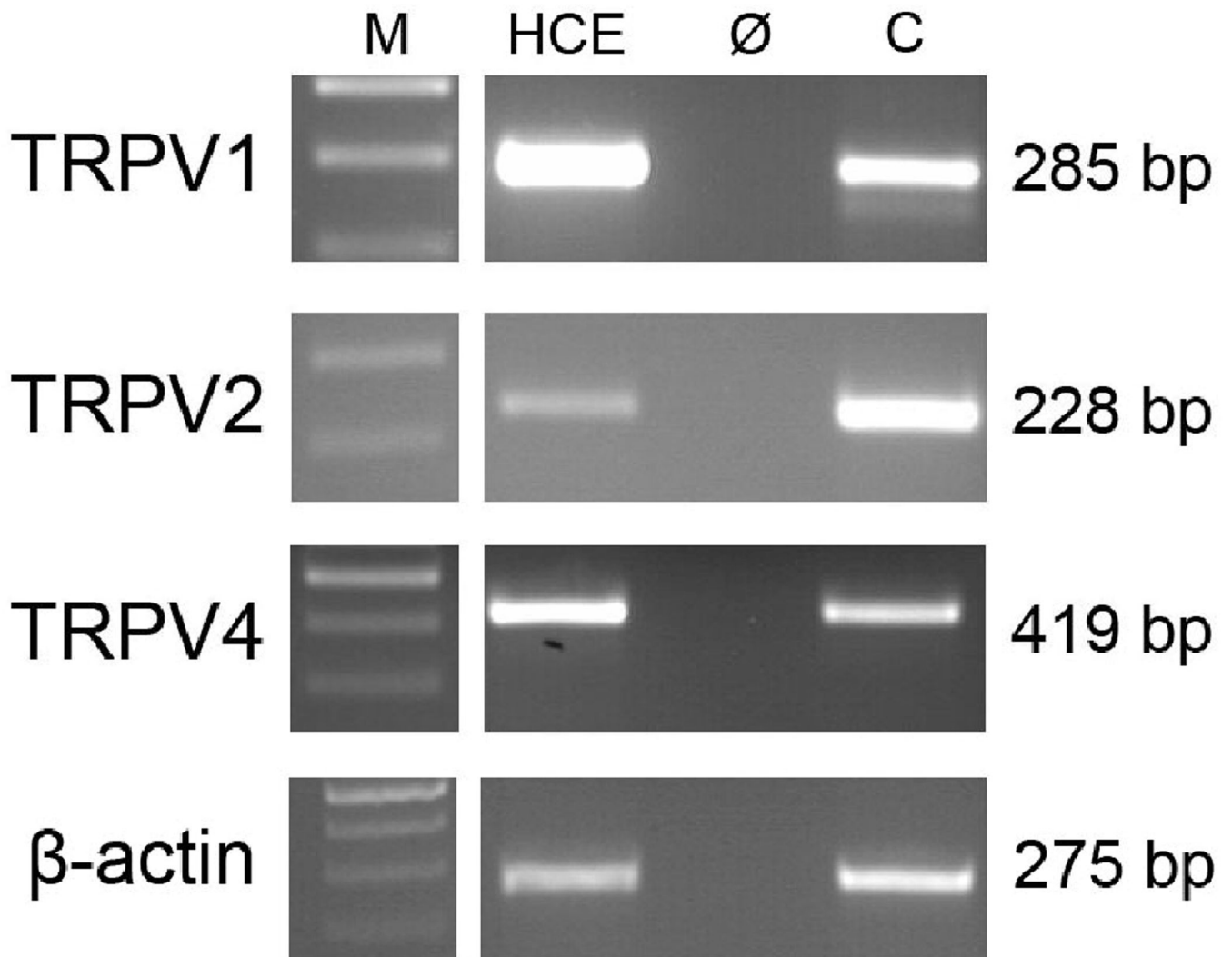
**Figure 2. RT-PCR analysis of functional expression of TRPV channels in cultivated human corneal epithelial cells (HCEC)**

Conventional RT-PCR revealed TRPV1, TRPV2 and TRPV4 gene expression in cultivated HCEC. Resulting PCR products (TRPV1 285 bp, TRPV2 228 bp and TRPV4 419 bp) were visualized in ethidium bromide-stained 2% agarose gels. PCR control (Ø) was performed without reverse transcriptase during cDNA synthesis to exclude primer binding to genomic DNA. As positive control (C), cDNA from human brain was used. M, DNA Ladder. HCEC cDNA integrity/stability was validated based on invariant and level of expression of β-actin as a housekeeping gene (standard lab protocol).
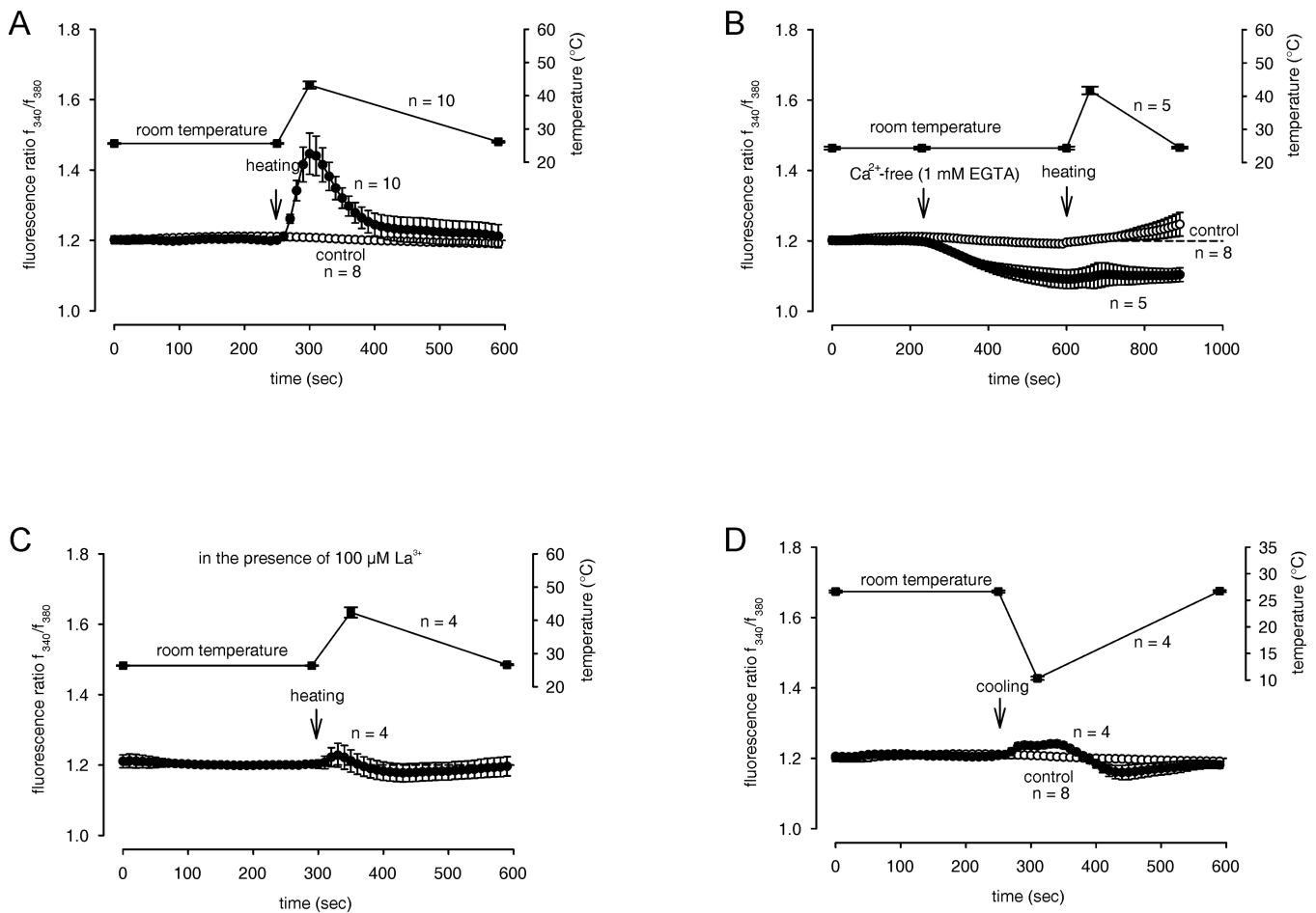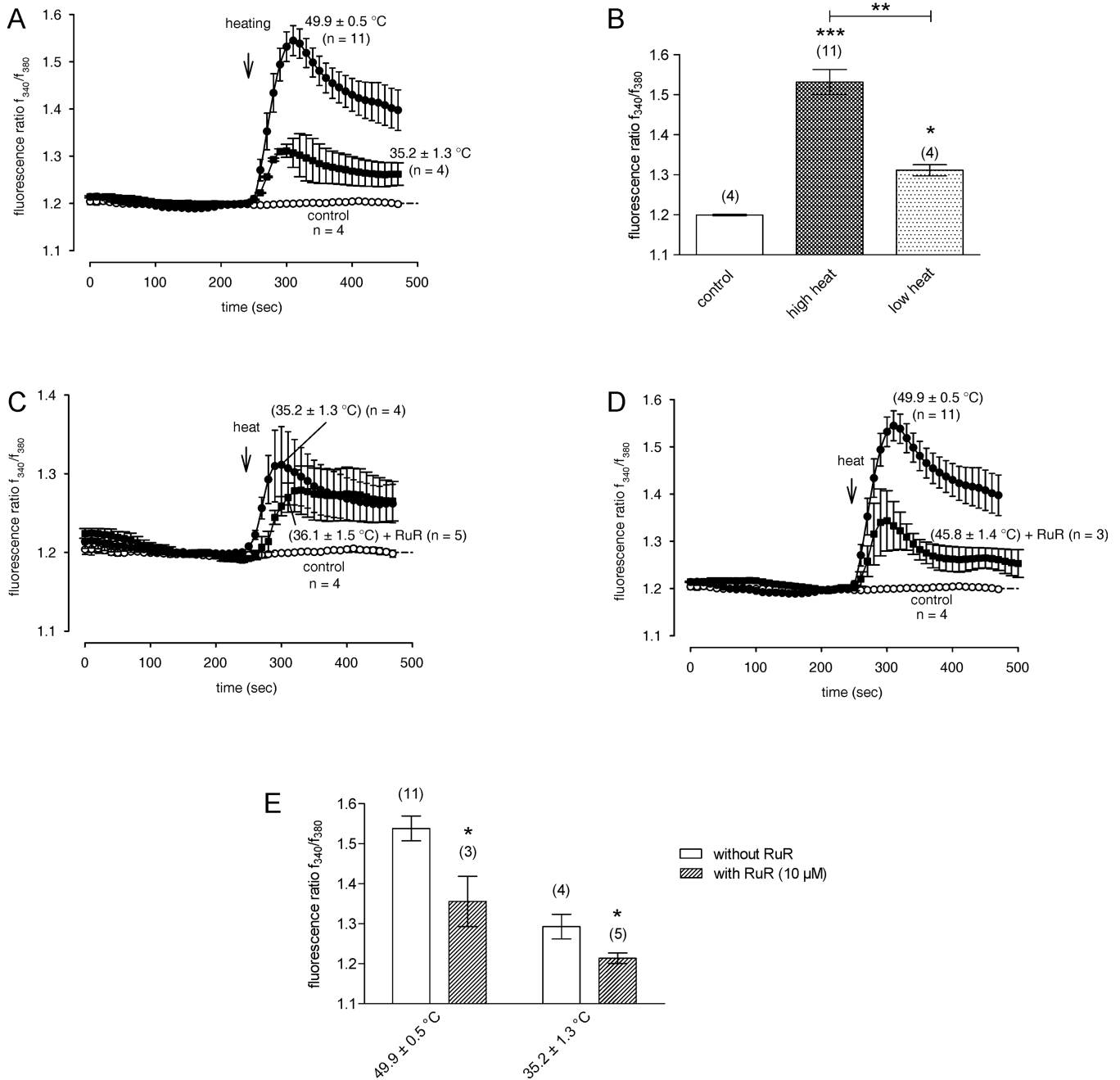
**Figure 3. Increase in cytosolic free Ca²⁺ concentration in HCEC caused by heat or cold exposure**
The thermal changes were carried out at the time points indicated by arrows. Data are mean ± SEM of 4 – 10 experiments. The corresponding temperature courses are shown above the Ca²⁺ traces. **(A)** Rise of bath solution temperature from 26 to over 43 °C resulted in Ca²⁺ elevation. Traces show intracellular Ca²⁺ measured of several neighboring cells with heat (filled circles) (n = 10) and without heat (open circles) (n = 8). **(B)** Following pre-incubation for 5 min with Ca²⁺-free bath solution containing 1 mM EGTA, heat (> 45 °C) (filled circles; n = 5) failed to induce an increase of Ca²⁺ above the Ca²⁺ base level (open circles; n = 8). **(C)** In the presence of the TRP channel blocker lanthanum chloride, La³⁺ (100 µM), the heat-induced Ca²⁺ increase was almost completely suppressed (n = 4). **(D)** Reduction of bath solution temperature from 25 to below 11 °C resulted in a completely changed Ca²⁺ response pattern (n = 4).
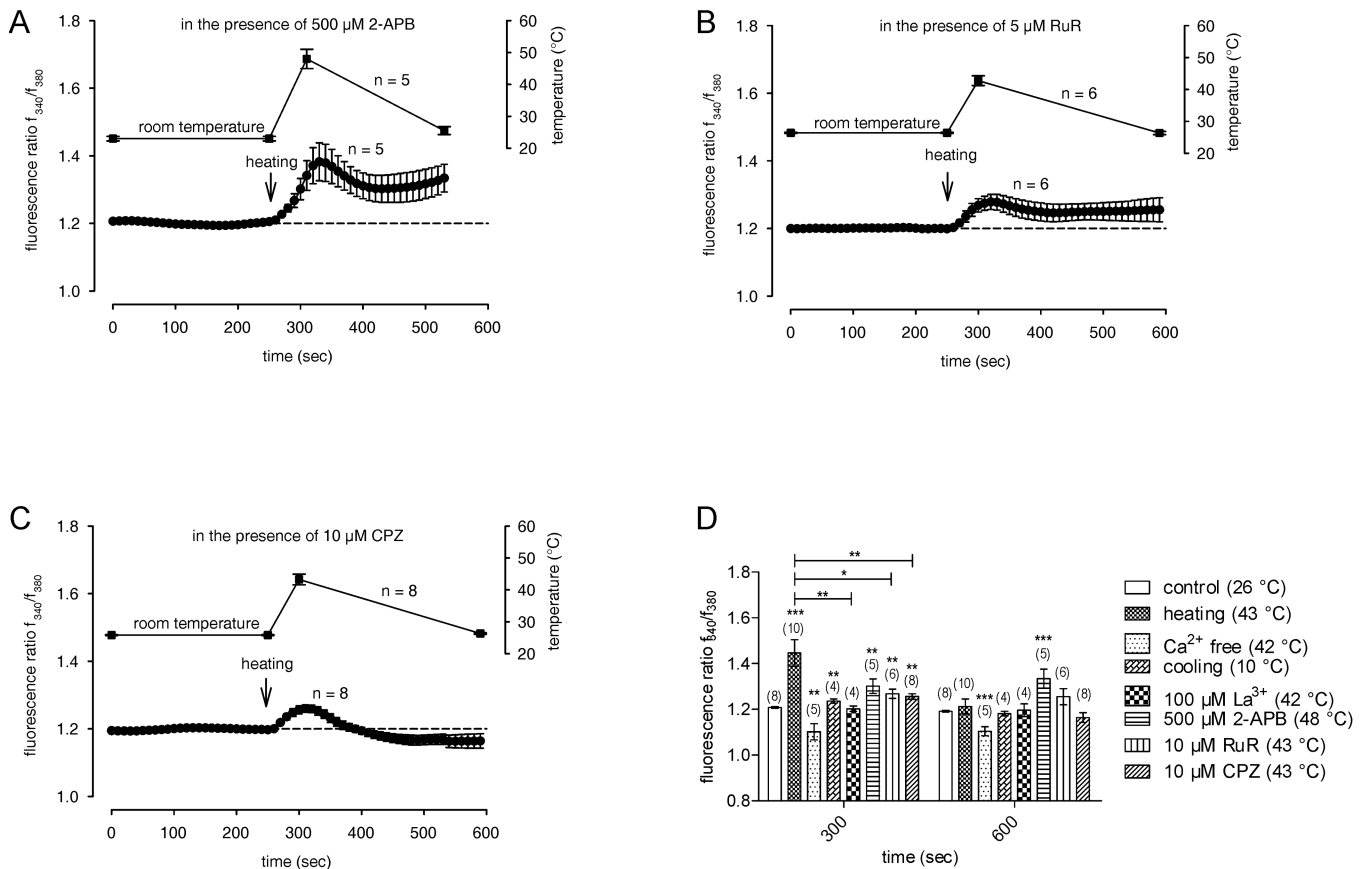
**Figure 4. Heat-induced increase in [Ca$^{2+}$]$_i$ in the presence of TRP channel modulators**
The thermal changes were carried out at the time points indicated by arrows. Data are mean ± SEM of 4 – 8 experiments. The corresponding temperature courses are shown above the Ca$^{2+}$ traces. **(A)** In the presence of the selective TRPV1-3 channel activator 2-aminoethoxydiphenyl borate, 2-APB (500 µM), the heat-induced Ca$^{2+}$ increase was not influenced (n = 5). **(B)** In the presence of the TRPV channel blocker ruthenium-red, RuR (10 µM), the heat-induced Ca$^{2+}$ increase was significantly suppressed (n = 6). **(C)** In the presence of the TRPV1 antagonist, CPZ (10 µM), the heat-induced Ca$^{2+}$ increase was significantly suppressed. **(D)** Summary of the experiments with La$^{3+}$, 2-APB, RuR, CPZ and Ca$^{2+}$-free solution in HCEC. The asterisks (*) indicate significant differences between controls (Ca$^{2+}$ base levels; n = 8) and the effect of TRP channel modulators on [Ca$^{2+}$]$_i$ and between the heat-induced increased Ca$^{2+}$ levels (n = 10) and the same effect in the presence of the TRP channel modulators (n = 4 – 8), respectively.

**Figure 5. TRPV1-3-induced Ca$^{2+}$ signaling in HCEC following fura2-loading and [Ca$^{2+}$]$_i$ monitoring using fluorescence cell imaging in a sodium- and potassium-free solution**

The reagent was added at the time points indicated by an arrow. Data are mean ± SEM of 4 – 12 experiments. **(A)** 2-APB (100 µM) (filled circles) activating TRPV1-3 induced Ca$^{2+}$ influxes. Recovery partially occurred to the Ca$^{2+}$ base level (n = 12). **(B)** The 2-APB-induced Ca$^{2+}$ increase was significantly reduced in the presence of RuR (10 µM) (n = 9). **(C)** Summary of the experiments with 2-APB in HCEC. The asterisks (*) indicate significant differences between controls (Ca$^{2+}$ base levels; n = 4) and the effect of 2-APB on [Ca$^{2+}$]$_i$ (n = 12) and between the 2-APB-induced increased Ca$^{2+}$ levels with and without RuR, respectively.

**Figure 6. Different increases in $[Ca^{2+}]_i$ induced by different levels of heat stimulation with and without the TRPV channel inhibitor RuR**

The thermal changes were carried out at the time points indicated by arrows. Data are mean ± SEM of 3 – 11 experiments. The corresponding mean heat stimulation temperature is noted near the $Ca^{2+}$ traces. (**A**) Rise of bath solution temperature from room temperature to nearly 50 °C resulted in more elevated $Ca^{2+}$ levels compared to those after low heat stimulation (35 °C). Traces show intracellular $Ca^{2+}$ levels measured from several neighboring cells with high heat stimulation (filled circles) (n = 11), low heat stimulation (filled quadrangles) (n = 4) and without heat (open circles) (n = 4). (**B**) Summary of the experiments with low and high heat stimulation in HCEC. The asterisks (*) indicate

significant differences between controls ($Ca^{2+}$ base levels; n = 4) and the effect of high heat stimulation on $[Ca^{2+}]_i$ (n = 11) and low heat-induced increased $Ca^{2+}$ levels (n = 4). **(C)** The low heat-induced $Ca^{2+}$ increase was significantly reduced in the presence of RuR at the beginning of the low heat response (10 µM) (n = 5). **(D)** The high heat-induced $Ca^{2+}$ increase was significantly reduced in the presence of RuR after the high heat response (n = 3). **(E)** Summary of the experiments with RuR after low and high heat stimulation in HCEC. The asterisks (*) indicate significant differences between the effect of RuR at high heat stimulation on $[Ca^{2+}]_i$ (n = 3 – 11) and low heat stimulation on $[Ca^{2+}]_i$ (n = 4 – 5).
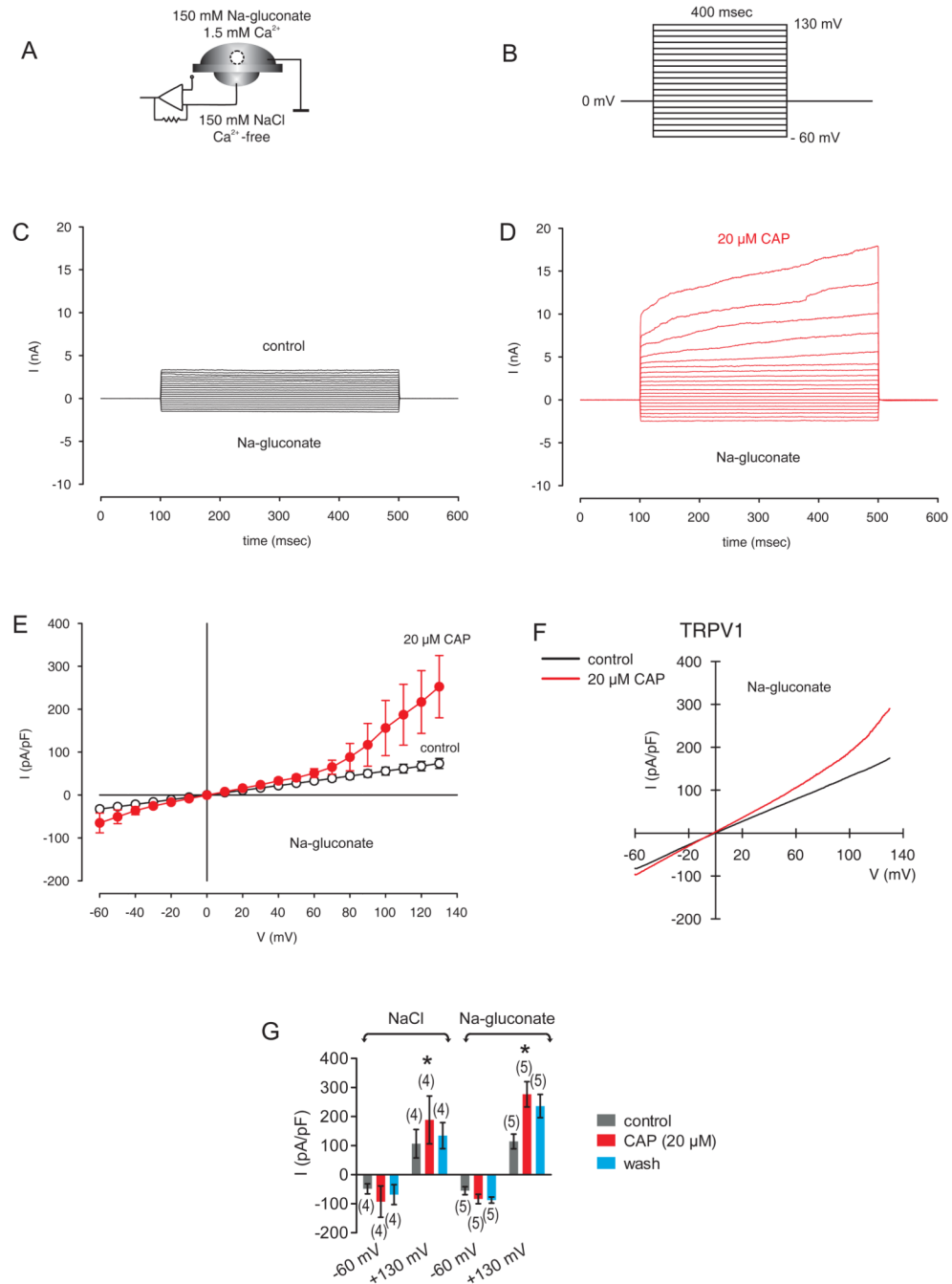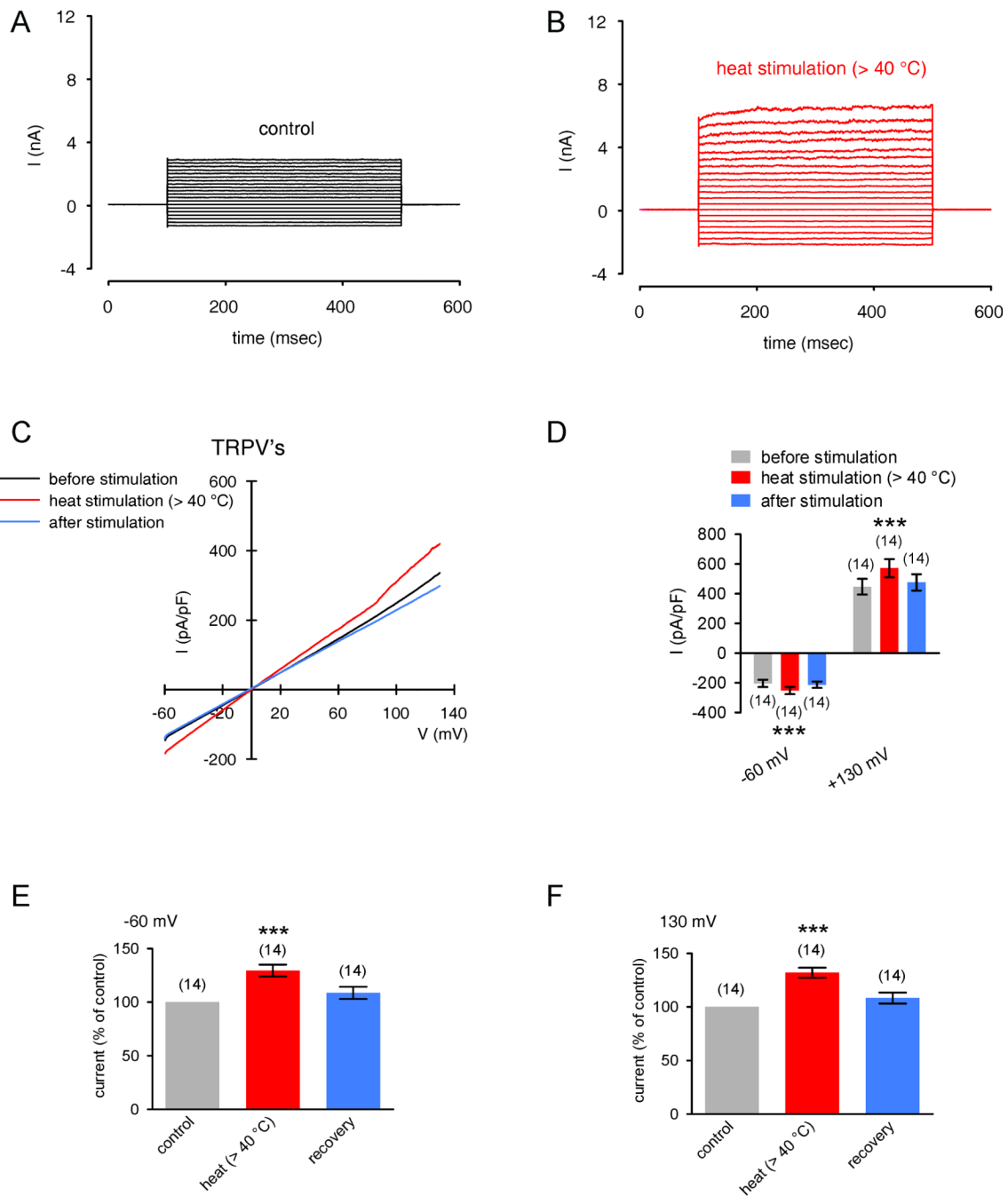
**Figure 7. Identification of CAP-activated non-selective cation channel currents**

**(A)** Experimental design (whole-cell configuration of the planar-patch clamp technique). Currents could be identified by their dependence on the permeating ion. Partial replacement of anions by a non-permeating ion (gluconate) is a frequently used identifier. **(B)** Voltage pulse protocol. Holding potential (HP) was set to 0 mV to avoid any voltage-dependent ion channel currents. **(C)** Non-selective cation channel currents induced by depolarization from −60 mV to 130 mV after establishing the whole-cell configuration (without leak current compensation). Possible anionic (chloride) outward currents were pharmacologically suppressed by withdrawal of the permeating ion. **(D)** Increased cation channel currents in the presence of CAP (20 μM). **(E)** Effect of CAP is summarized in a current/voltage plot (I–

V plot) (n = 3). For the current/voltage relation, maximal peak current amplitudes were plotted against the voltage (mV). The currents were normalized to capacitance to obtain current density (pA/pF). The upper trace (red filled circles) was obtained in the presence of 20 µM CAP and the lower trace (open circles) without CAP. CAP-induced increases in non-selective cation channel outward currents at potentials above +60 mV were discernable. **(F)** Original traces of CAP activated TRPV1 channel responses to voltage ramps from −60 mV up to +130 mV (without leak current compensation) in the whole-cell configuration of the planar patch-clamp technique. Currents are shown before application (black) and during application of CAP (20 µM, red). The currents were normalized to capacitance to obtain current density (pA/pF). **(G)** Summary of the experiments with CAP in the presence of NaCl versus Nagluconate in the external solution. The asterisks (*) indicate statistically significant differences between outward currents with and without CAP (n = 4 – 5; $p < 0.05$; paired tested). No differences of CAP-induced outward currents could be registered between NaCl and Na-gluconate in the external solution (n = 4 – 5; $p > 0.05$; unpaired tested).

**Figure 8. Thermo-TRPs in HCEC**

**(A)** Maximal cation channel currents induced by depolarization from 0 mV to 130 mV after establishing the whole-cell configuration of the planar patch-clamp technique (control). **(B)** Same currents after heat stimulation above 40 °C. Heat induced increases in non-selective cation channel outward and inward currents were discernable. **(C)** Original traces of heat activated TRPV channel responses to voltage ramps from −60 mV up to +130 mV (no leak current compensation). Heat induced currents are shown before stimulation (black), during the stimulation by application of heated solution (> 40 °C, red), and after stimulation (blue). The currents were normalized to capacitance to obtain current density (pA/pF). **(D)** Comparison of inward and outward current densities with and without heat stimulation at

−60 mV and +130 mV. Color bars show mean inward and outward current densities at temperatures above 40 °C (red) and after stimulation (blue). Gray bars represent mean current densities at 20 °C (before stimulation). The asterisks (****) denote significant increase by heat stimuli (n = 14; p < 0.005; paired tested). **(E)** – **(F)** Summary of the experiments with heat stimulation. The asterisks (***) indicate statistically significant differences between controls and heat stimulation at −60 mV and 130 mV (n = 14; p < 0.005; paired tested).
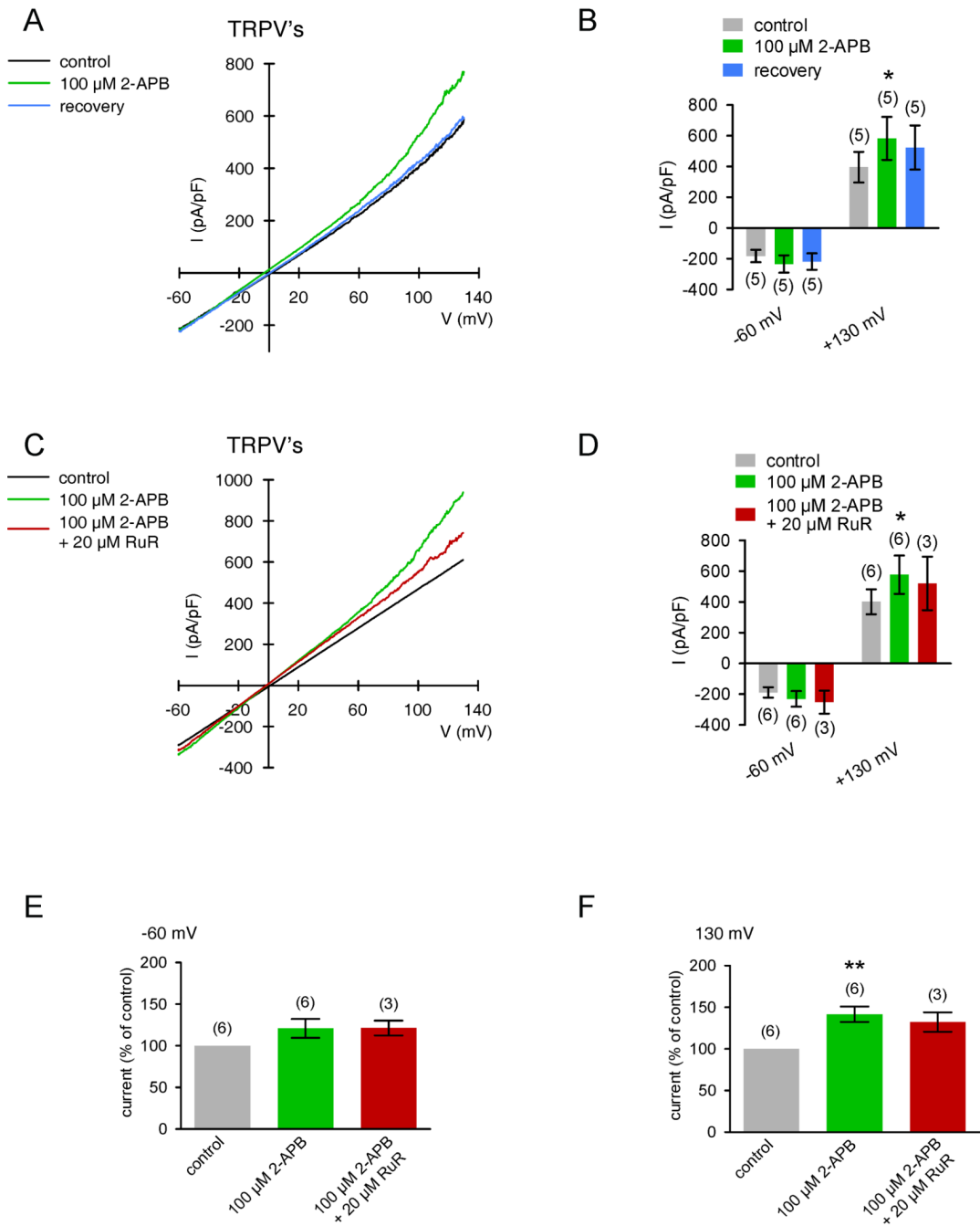
**Figure 9. 2-APB-induced increases of non-selective cation channel currents**
(**A**) Original traces of 2-APB activated TRPV channel responses to voltage ramps from −60 mV up to +130 mV (no leak current compensation) in the whole-cell configuration of the planar patch-clamp technique. Currents are shown before application (black), during application of 2-APB 100 μM, green), and after washout (blue). The currents were normalized to capacitance to obtain current density (pA/pF). (**B**) Comparison of inward and outward current densities with and without 2-APB at −60 mV and +130 mV (n = 5). Color bars show mean inward and outward current densities with 2-APB (green) and after washout (blue). Gray bars represent mean current densities without 2-APB (control). The asterisk (*) denote significant increase of outward currents by 2-APB (n = 5; p < 0.05; paired tested).

**(C)** – **(D)** Similar experiments as shown in (A) and (B) (n = 6), but 20 µM ruthenium-red (RuR) was added in the presence of 2-APB instead of washout (n = 3; red-brown trace and bars). **(E)** – **(F)** Summary of the experiments with 2-APB and RuR. The asterisks (**) indicate statistically significant differences between controls and 2-APB at 130 mV (n = 6; p < 0.01; paired tested). Note that RuR suppressed 2-APB induced increases of outward currents (n = 3; p < 0.05; paired tested).
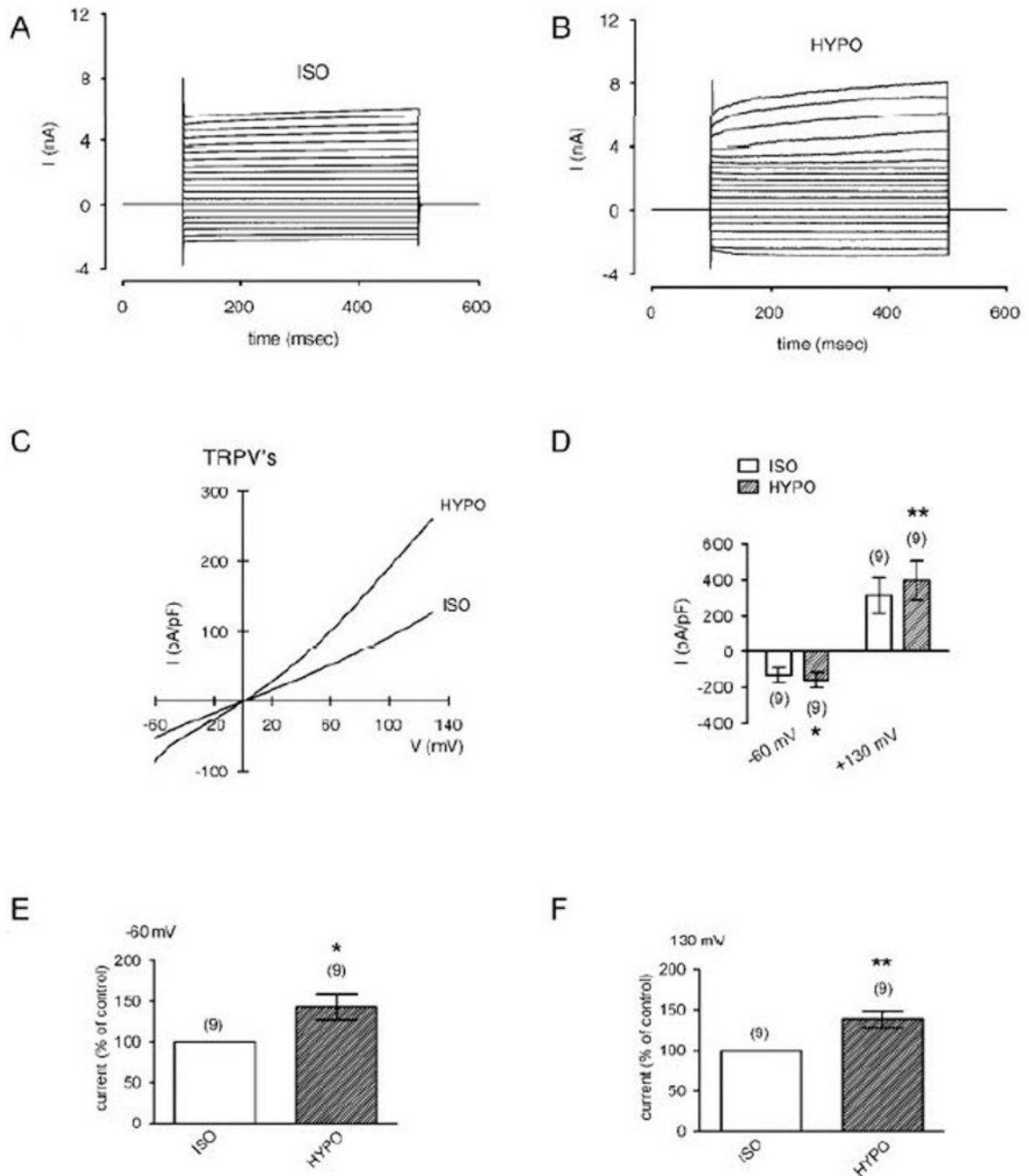
**Figure 10. Activation of TRPV4 by hypotonic challenge in HCEC**
**(A)** Maximal cation channel currents induced by depolarization from 0 mV to 130 mV after establishing the whole-cell configuration of the planar patch-clamp technique in an isotonic solution (ISO). **(B)** Same currents after changing to a hypotonic solution (25 %) (HYPO). Hypotonic stress induced increases in non-selective cation channel outward and inward currents were discernable. **(C)** Original traces of hypotonic stress activated TRPV channel responses to voltage ramps from −60 mV up to +130 mV (no leak current compensation). Currents are shown in the presence of an isotonic solution (ISO) and change to a hypotonic solution (HYPO). The currents were normalized to capacitance to obtain current density (pA/pF). **(D)** Comparison of inward and outward current densities between isotonic and

hypotonic solution at −60 mV and +130 mV. Filled bars show mean inward and outward current densities under hypotonic stress (25 %). Open bars represent mean current densities with isotonic solution (control). The asterisks (**) denote significant increase by hypotonic challenge (n = 9; p < 0.01; paired tested). **(E)** – **(F)** Summary of the experiments with hypotonic challenge. The asterisks (*) and (**) indicate statistically significant differences between currents at isotonic and hypotonic solution at −60 mV and 130 mV (n = 9; p < 0.05 and 0.01 resp.; always paired tested).